Carbon 108 (2016) 343–350

Contents lists available at ScienceDirect

Carbon

journal homepage: www.elsevier.com/locate/carbon

Graphdiyne-supported single-atom Sc and Ti catalysts for high-efficient CO oxidation

Zheng-Zhe Lin

School of Physics and Optoelectronic Engineering, Xidian University, Xi'an 710071, China

ARTICLE INFO

Article history:
Received 29 April 2016
Received in revised form
30 June 2016
Accepted 18 July 2016
Available online 19 July 2016

ABSTRACT

Single-layer graphdiyne was proposed as substrate for single-atom Sc and Ti catalysts with much larger binding energy and higher thermal migration barrier than graphene. By density functional theory calculations, the electronic properties, thermal stabilities and catalytic abilities of Sc and Ti adatoms on single-layer graphdiyne were theoretically investigated. The results indicate that the **C** sites on graphdiyne surface are the most stable binding sites for Sc and Ti adatoms. The high migration barrier prevents the aggregation of Sc and Ti adatoms on graphdiyne surface. On graphdiyne-Sc or graphdiyne-Ti, CO could be catalytically oxidated by a four-step reaction. The reaction is both energetically and kinetically favorable with low potential barriers. Overall, Sc and Ti adatoms on single-layer graphdiyne would be excellent catalysts for CO oxidation.

1. Introduction

Substrate-supported noble metal nanoparticles are widely used in heterogeneous catalysis. For a long time, people have insisted in minimizing the size of noble metal nanoparticles to enhance the performance of catalysts. Since low-coordinated metal atoms often act as catalytic active sites, the catalytic activity usually increases with decreasing size of metal nanoparticles. The ultimate size limit for metal particles is the single-atom catalyst, which contains isolated metal atoms scattered on supports. Single-atom metal catalysts anchored to substrate maximize the efficiency of metal atom use and exhibit more superior catalytic activity than conventional metal nanoparticles in many important chemical reactions [1–4]. In recent years, people have focused on searching for anti-CO catalysts or effective techniques to transform CO into other molecules [5–12]. As separate and highly active centers, single-atom catalysts have the potential to directly transform CO into other molecules. For example, single-atom Pt_1/FeO_x catalyst shows a high catalytic efficiency to CO oxidation and preferential oxidation of CO in H_2 [1], and single-atom Ir_1/FeO_x catalyst shows remarkable performance in the water gas shift reaction ($CO + H_2O \rightarrow CO_2 + H_2$) [3]. Single Au atom embedded in graphene monovacancy was also theoretically predicted as highly efficient catalyst for CO oxidation [13]. The success in single-atom catalysts open a new way to efficiently removing the CO contamination. Meanwhile, the corresponding theoretical research on understanding the catalytic mechanism could provide guidance for future applications of single-atom catalysts.

The high surface energy promotes the aggregation of metal nanoparticles or single-atom catalysts. Appropriate substrates that strongly interact with single-atom catalysts could prevent the aggregation. On the other hand, to enhance the catalytic efficiency, it is beneficial to spread single-atom catalysts on substrates with large specific surface area. In recent years, the rapid development on graphene [14–18], molybdenum disulfide [19–21] and other two-dimensional materials provides more choices of substrates for stabilizing single-atom catalysts. With large specific surface area, two-dimensional materials are advantageous to use them as the substrates. However, people found that the interactions between graphene and metal atoms are rather weak because the strong π bonds in pristine graphene are rather chemically inert. Theoretical calculation showed that the adsorption energies of transition adatoms on graphene are about 1eV [22–25], and the migration barriers of transition adatoms on graphene are about 0.2–0.8 eV, indicating that the transition adatoms would migrate on graphene surface at room temperature [26]. Graphyne and its family, a series of hypothetical two-dimensional carbon allotropes that were predicted about twenty years ago [27–29], have been considered as possible substrates with large binding energies to single-atom catalysts. The graphyne sheets are composed of sp^2-hybridized hexagonal C rings and *sp*-hybridized −C≡C− linkages, in which the

E-mail address: linzhengzhe@hotmail.com.

http://dx.doi.org/10.1016/j.carbon.2016.07.040
0008-6223/

additional p_x-p_y π/π^* states in the −C≡C− bonds could rotate towards any direction perpendicular to the bonds. This makes it possible for the π/π^* states to all point towards the single-atom catalyst and lead to large binding energy to metal atoms. In 2010, graphdiyne has been successfully synthesized on the surface of copper via a cross-coupling reaction using hexaethynylbenzene [30]. Recent theoretical studies mainly concentrated on the basic electronic properties of graphdiyne [31–33] and other hypothetical graphyne-like structures [34–37]. A recent report [38] has suggested graphdiyne as catalyst for CO oxidation. Meanwhile, our previous works have suggested the large binding energy of single-layer graphdiyne sheet to single metal atoms [39] and small Pt nanoparticles [40]. Thus single-atom catalysts anchored to single-layer graphdiyne sheet would be promising thermally stable catalysts.

In this work, density functional theory (DFT) calculations were employed to investigate the thermal stabilities and catalytic abilities of Sc and Ti adatoms on single-layer graphdiyne. The binding ability of single-layer graphdiyne to Sc and Ti adatoms was found stronger than graphene. The migration barriers of Sc and Ti adatoms on graphdiyne are high enough for preventing the aggregation of these adatoms. Then, minimum-energy path (MEP) calculations were performed to investigate the catalytic CO oxidation by Sc and Ti adatom. According to the results, in O_2 ambient CO could be catalytically oxidated on Sc or Ti adatoms via a four-step reaction. The reaction was found both thermodynamically and kinetically favorable, with stable reaction intermediates and low potential barrier. Overall, with both high thermal stability and catalytic ability, Sc and Ti adatoms on single-layer graphdiyne should be excellent catalysts for removing the CO contamination.

2. Computational details

DFT calculations were performed using the SIESTA code [41]. The norm-conserving pseudopotentials were generated using the improved Troullier-Martins scheme [42]. The generalized gradient approximation (GGA) according to Perdew-Burke-Ernzerhof (PBE) [43] was employed for both the generation of the pseudopotentials and the exchange-correlation functional. Grimme's DFT-D2 correction [44] was employed for evaluating dispersion interactions. Non-linear exchange-correlation core corrections were used. The double-ζ plus polarization (DZP) basis set was used and the grid mesh cutoff was set 250 Ry. All the calculations were performed with spin-polarization. The convergence of the total energy was considered to be achieved until two iterated steps with energy difference less than 10^{-5} eV.

Single-layer graphdiyne was simulated by a repeated slab model with 2 × 2 supercell. The replicas of graphdiyne layers were separated by a vacuum layer of 20 Å. Geometries were fully relaxed until the Hellmann-Feynman forces were below 0.01 eV/Å. The Brillouin zone was sampled by using a 2 × 2 × 1 Monkhorst-Pack grid [45], while the calculations for the density of states (DOS) were performed by using a 8 × 8 × 1 Monkhorst-Pack grid.

The binding energy of a metal adatom M on graphdiyne is defined as

$$E_b = E(g) + E(M) - E(g-M), \quad (1)$$

where E(g), E(M) and E(g-M) denote the potential energies of free-standing graphdiyne, free M atom and the graphdiyne-M system, respectively. When a molecule is adsorbed on the graphdiyne-M system, the molecular binding energy is defined as

$$E_b = E(g-M) + E(mol) - E(g-M-mol), \quad (2)$$

where E(g–M), E(mol) and E(g–M–mol)) denote the potential energies of the graphdiyne-M system, free molecule and the graphdiyne-M-molecule system, respectively.

To find the minimum-energy path (MEP) and the corresponding potential barrier E_0 for metal adatom diffusions and catalytic reactions, the climbing image nudged elastic band (CINEB) method [46–48] was used. Five images were inserted in between two stable states, and the spring constant between adjacent images was 0.1 eV/Å. The geometric optimization and the search for the transition state (TS) were verified by means of frequency calculations. To account for electronic exchange in higher accuracy and obtain the precise value of potential barrier, the hybrid PBE0 functional [49] was employed to calculate the total energies of stable states and TSs. The PBE0 calculations were performed using the projector-augmented wave (PAW) method [50,51] as implemented in the VASP package [52,53] with a plane-wave energy cutoff of 400 eV. The correction on potential barrier was reckoned by the calculations performed at the level of both PBE and PBE0.

3. Results and discussion

3.1. Free-standing graphdiyne

Before going to our results, we first present the structure of free-standing graphdiyne. The primitive cell of graphdiyne (enclosed by dashed lines in Fig. 1(a)) contains 18 C atoms, including 6 C atoms in the hexagonal ring with sp^2 hybridization and 12 C atoms in the linear acetylenic chains with *sp* hybridization. The optimized lattice constant $a_0 = 9.51$ Å is in good agreement with the value of 9.48 Å calculated using the projector-augmented-wave method [31]. As shown in Fig. 1(a), the C–C bond length in the hexagon is 1.43 Å and the C–C bond lengths in the acetylenic linkages are 1.40, 1.25 and 1.35 Å, presenting alternating single and triple bonds. Furthermore, the calculation results show the semiconductor feature of graphdiyne with a direct band gap of 0.45/1.53 eV at the level of PBE/PBE0, respectively, in good agreement with the PBE value 0.46 eV in Ref. [31]. A recent report [38] has suggested free-standing graphdiyne as catalyst for CO oxidation. However, according to our calculation, the barrier E_0 = 1.73 eV (at the level of PBE) for O_2 adsorption on free-standing graphdiyne is higher than the barrier of CO catalytic oxidation on Sc or Ti adatom on graphdiyne (see Sec. 3.4).

3.2. Sc and Ti adatoms binding on graphdiyne

To investigate the binding of Sc and Ti adatoms on 2 × 2 graphdiyne supercell, three possible binding sites are considered as the corner (**C**) site of the acetylenic ring, the hollow (**H1**) site above the center of the hexagonal ring, and the hollow (**H2**) site in the center of the acetylenic ring. The area of graphdiyne supercell is large enough to avoid the interactions between the replicas of adatoms.

According to the calculation of binding energy E_b, the **C** and **H1** sites are stable binding sites for Sc and Ti adatoms, while the **H2** site is not a stable site because the adatoms gradually move from **H2** to **C** in the geometry relaxation. The **C** and **H1** sites were verified as stable binding sites using frequency calculations. For Sc and Ti adatoms, the binding energy E_b(**C**) on the **C** site (6.07/5.27 and 6.43/6.09 eV at the level of PBE/PBE0, each respectively) is much larger than the binding energy E_b(**H1**) on the **H1** site (3.79/and 4.07/eV at the level of PBE/PBE0, each respectively) (Table 1). Therefore, the **C** site should be the most stable binding site for Sc and Ti adatoms on

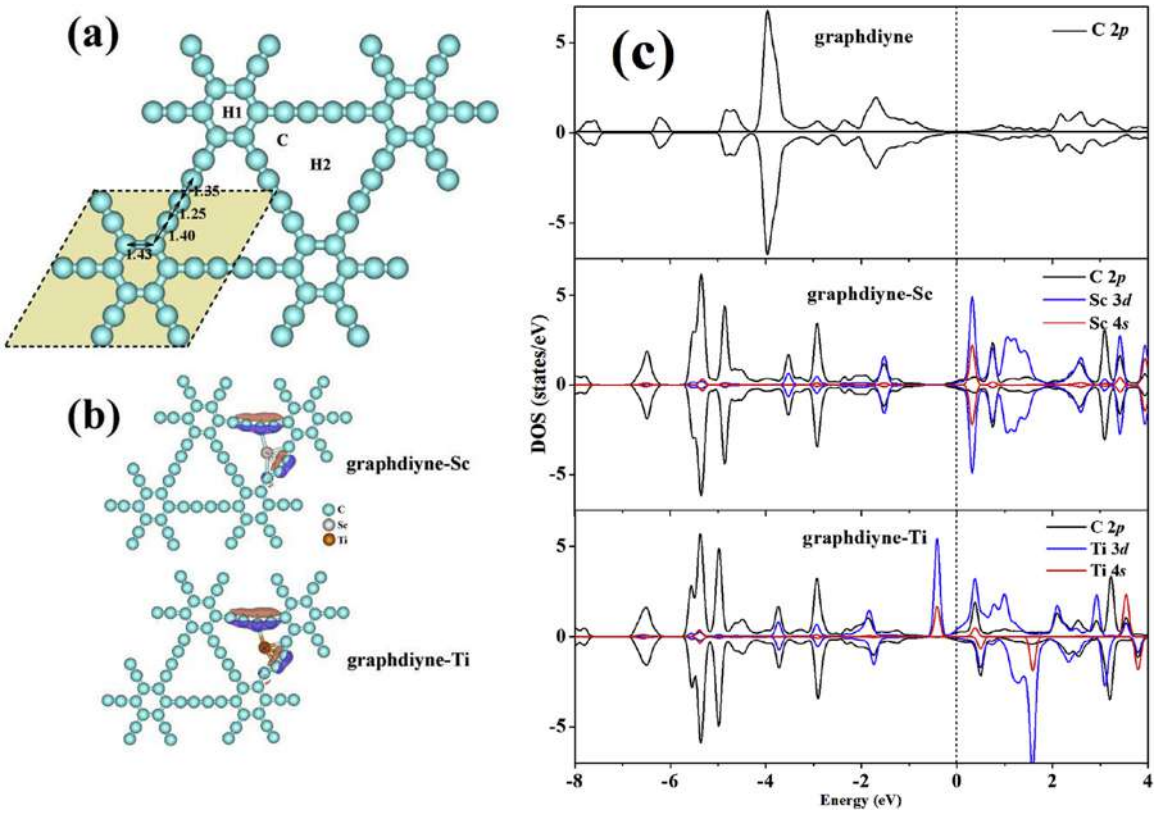

Fig. 1. (a) Atomic configuration of free-standing graphdiyne sheet. The primitive cell is enclosed by dashed lines. The C–C bond lengths (in Å) are indicated. **C**, **H1** and **H2** are the considered binding sites for Sc and Ti adatoms. (b) The geometric structures of Sc and Ti adatoms on graphdiyne sheet. Isosurfaces of charge redistribution with values of ±0.05e/Å^3 (blue/red respectively) are shown. (c) The positive and negative LDOS denote the spin-up and spin-down states, respectively. The vertical dashed line indicates the Fermi level. (A colour version of this figure can be viewed online.)

Table 1
The binding energy E_b (in eV) of Sc and Ti adatoms on the **C** and **H1** sites of graphdiyne, and the diffusion barrier E_0 (in eV) between these sites. All the values are calculated at the level of PBE/PBE0.

Adatom	Binding energy (PBE/PBE0)		Diffusion barrier (PBE/PBE0)		
	E_b(C)	E_b(H1)	E_0(C→C)	E_0(C→H1)	E_0(H1→C)
Sc	6.07/5.27	3.79/3.15	2.19/1.95	2.62/2.55	0.34/0.43
Ti	6.43/6.09	4.07/4.06	1.73/2.07	2.37/2.63	0.55/0.60

graphdiyne. Fig. 1(b) presents the atomic configurations of Sc and Ti located on the **C** site of graphdiyne, both showing distorted planar structures. In the distorted planar structures, the Sc/Ti adatom locate in the same plane with graphdiyne sheet, with bond lengths from Sc/Ti to nearest C atoms in the range of 2.2–2.5/2.1–2.5 Å, respectively. The electronic charge redistribution (Fig. 1(b)) shows bonding of Sc/Ti with nearest C atoms. The binding energy E_b(**C**) of Sc and Ti on graphdiyne (6.07 and 6.43 eV at the level of PBE, respectively) is larger than or close to V, Cr, Mn, Fe, Co and Ni on graphdiyne (5.92, 2.58, 2.82, 5.38, 6.09 and 6.75 eV at the level of PBE, respectively). Hubbard PBE + U correction provides more precise E_b(**C**) for V, Cr, Mn, Fe, Co and Ni on graphdiyne [54], which is in the range of 1–3 eV. It can be judged that in the first row of transition metals, Sc and Ti have almost the most stable binding on graphdiyne surface.

Furthermore, it is worth noting that the values E_b(**C**) of Sc and Ti adatoms (6.07/5.27 and 6.43/6.09 eV at the level of PBE/PBE0, each respectively) on graphdiyne are much larger than the binding energies of Sc and Ti on graphene (1.35/0.96 and 1.84/1.95 eV at the level of PBE/PBE0, each respectively, according to our calculation with 5 × 5 graphene supercell), suggesting that the stability of graphdiyne-Sc/Ti are much higher than that of graphene-Sc/Ti. Previous works [22,23,55] also predicted that the binding energies of Sc and Ti on graphene are less than 2 eV, and the binding energies of Fe, Co, Ni, Cu, Pt on graphdiyne (4–7 eV) [39,54] were also predicted to be much larger than their corresponding binding energies on graphene [22–26,55,56]. In general, transition metal adatoms on graphdiyne should have significantly larger binding energies because of the p_x-p_y π/π^* states existing in the acetylenic linkages of graphdiyne sheet. Such hybridization enables the p_x-p_y π/π^* states to rotate towards any direction perpendicular to the acetylenic linkages, thus making it possible for the p_x-p_y π/π^* states to point to the metal adatom. In graphyne, similar effect has been also revealed [54,57–59], which leads to large binding energies to transition metal adatoms. For example, the binding energies of Pt, Ir, Pd, Rh, Ru and Fe adatoms on graphyne are 4.3, 5.2, 2.7, 3.7, 4.6 and 5.0 [57,58], respectively. Overall, graphdiyne would be a promising substrate for transition metal single-atom catalysts.

To gain more insight into the electronic structure, the spin-polarized local DOS (LDOS) was projected on the 3*d* and 4*s* orbitals of the Sc/Ti adatom as well as the 2*p* orbitals of five nearest C atoms. As shown in Fig. 1(c), the peak values of the LDOS of the Sc/Ti 3*d* orbitals below the Fermi level get close to some peak values of the C 2*p* orbitals. This suggests a strong 2*p*-3*d* bonding between C atoms and Sc/Ti adatom. The spin-up and spin-down DOS of the Sc 3*d* orbitals are symmetric due to the quenching of the spin magnetic moments, while those of the Ti 3*d* orbitals are asymmetric. Importantly, a large number of unoccupied Sc/Ti 3*d* orbitals near the Fermi level play a critical role in adsorbing and activating the

incoming adsorbates.

Single metal adatoms may have high mobility on a substrate and prefer to form a metal cluster. To understand the thermal diffusion of the adsorbed Sc and Ti adatoms on graphdiyne, the MEPs and corresponding potential barriers E_0 of the migrations between the binding sites (Table 1) were calculated to predict the durability of Sc and Ti adatoms on graphdiyne. According to the Arrhenius expression for the rate constant, the typical time scale of a migration with barrier E_0 can be estimated from $\tau = \omega^{-1}\exp(E_0/kT)$, where T is the temperature and $k = 8.617 \times 10^{-5}$ eV/K is the Boltzmann constant. The empirical parameter ω is roughly estimated to be 10^{13} s^{-1} [60,61]. For Sc and Ti adatom diffusing from one **C** site to another neighboring **C** site, with barrier $E_0(\mathbf{C}\rightarrow\mathbf{C}) = 2.19/1.95$ and 1.73/2.07 eV calculated at the level of PBE/PBE0, the typical time scale τ for this event at $T = 300$ K is $2 \times 10^{16}/2 \times 10^{12}$ and $4 \times 10^{8}/2 \times 10^{14}$ years, each respectively. As for the diffusion from the **C** site to the nearest **H1** site, the barrier $E_0(\mathbf{C}\rightarrow\mathbf{H1}) = 2.62/2.55$ and 2.37/2.63 eV for Sc and Ti at the level of PBE/PBE0, each respectively, is higher than $E_0(\mathbf{C}\rightarrow\mathbf{C})$, indicating that the diffusion rate from **C** to **H1** is even much slower than the rate of **C**→**C**. However, the barriers $E_0(\mathbf{H1}\rightarrow\mathbf{C}) = 0.34/0.43$ and 0.55/0.60 eV of the inverse process of Sc and Ti at the level of PBE/PBE0, each respectively, are rather low, corresponding to a diffusion time $\tau = 5 \times 10^{-8}/2 \times 10^{-6}$ and $2 \times 10^{-4}/1 \times 10^{-3}$ s from **H1** to **C** at $T = 300$ K. So, a Sc or Ti adatom staying at the **H1** site would instantaneously migrate to the **C** site. Overall, the above results suggest that the Sc and Ti adatoms adsorbed on graphdiyne sheet should be stably bound on the **C** site, without diffusion or aggregation at room temperature.

3.3. CO and O_2 binding on graphdiyne-Sc and graphdiyne-Ti

As the prerequisite for CO oxidation, the binding of CO and O_2 on graphdiyne-Sc and graphdiyne-Ti was investigated before exploring the catalytic mechanism. Geometry relaxations for various initial guess were performed to find the configurations of CO and O_2 on Sc/Ti adatom. The geometry with the lowest total energy was denoted as the most stable configuration. Since electron transfer may happen between CO/O_2 and Sc/Ti adatom as the binding center, LDOS was projected on the 3*d* and 4*s* orbitals of the Sc/Ti adatom as well as the CO/O_2 molecule to investigate the bonding.

Both CO and O_2 are found to strongly interact with graphdiyne-Sc and graphdiyne-Ti. The upper panels in Fig. 2 (a) and (c) present the structures of graphdiyne-Sc·CO and graphdiyne-Ti·CO, respectively. In both structures, CO molecule is bound with the C atom bonding to the Sc/Ti atom. The middle panels in Fig. 2 (a) and (b) present the structures of graphdiyne-Sc·O_2 and graphdiyne-Ti·O_2, respectively. In both structures, the two O atoms of O_2 molecule all bond to the Sc/Ti atom. The following data in this section were all calculated at the level of PBE. In these most stable binding configurations, the binding energy $E_b(O_2|M) = 2.73$, 3.69 eV on graphdiyne-M is larger than $E_b(CO|M) = 1.17$, 1.60 eV for both M = Sc, Ti, respectively (Table 2). Similar results ($E_b(O_2|M) > E_b(CO|M)$) were also found for single-atom Ir, Rh and Ru catalysts on graphyne [57]. So, O_2 molecule is more likely to be adsorbed on Sc or Ti adatom than CO. At $T = 300$ K, the typical time scale of O_2 molecule leaving the Sc/Ti adatom could be roughly estimated as $\tau = \omega^{-1}\exp(E_b(O_2|M)/kT) = 7 \times 10^{32}/1 \times 10^{49}$ s, respectively, indicating the strong bondage of Sc and Ti adatoms to O_2 molecule. The binding of O_2 is still strong even in the existence of a preabsorbed CO molecule. For M = Sc/Ti, the binding energy $E_b(O_2|M{\cdot}CO) = 2.47/2.75$ eV of O_2 on graphdiyne-M·CO is close to $E_b(O_2|M) = 2.73/3.69$ eV on graphdiyne-M without CO, respectively. Overall, the large binding energy makes the preadsorption of O_2 on the metal adatom, providing a prerequisite for CO oxidation.

To understand the bonding between the metal adatom M = Sc/Ti and molecule (CO/O_2), the LDOS of graphdiyne-M·CO and graphdiyne-M·O_2 was projected on the 3*d* and 4*s* orbitals of M and CO/O_2 (Fig. 2 (c) and (d)). For graphdiyne-M·CO, although the molecular orbital energies of CO is lowered by M, the antibonding $2\pi^*$ orbital is still above the Fermi level (the upper panels of Fig. 2 (c) and (d)). So, the C–O bond length in graphdiyne-M·CO (1.16 and 1.17 Å for M = Sc and Ti, respectively) is close to the bond length in free CO molecule (1.16 Å). In contrast, for graphdiyne-M·O_2 (the lower panels of Fig. 2 (c) and (d)), the electrons of M are injected into the antibonding $2\pi^*$ orbital of O_2, with the energy of $2\pi^*$ orbital below the Fermi level. Hirshfeld charge analysis revealed that the O_2 molecule obtains 0.38/0.32 *e* from the metal adatom M = Sc/Ti, respectively. As a result, the O–O bond length in graphdiyne-M·O_2 (1.46/1.45 Å for M = Sc/Ti, respectively) is obviously more elongated than the bond length in free O_2 molecule (1.24 Å). The electron injection into O_2 molecule weakens the O–O bond, which is advantageous to CO catalytic oxidation.

3.4. CO catalytic oxidation on graphdiyne-Sc and graphdiyne-Ti

In this section, the reaction mechanism of CO oxidation on graphdiyne-Sc and graphdiyne-Ti was investigated. Generally, there are two well-established mechanisms for heterogeneous catalysis, namely the Langmuir-Hinshelwood (LH) and Eleye-Rideal (ER) mechanisms. The LH mechanism involves the adsorption of two kinds of reactant molecules. By contrast, in the ER mechanism one gas-phase molecule directly reacts with another preadsorbed molecule. For the LH reactions on graphdiyne-Sc and graphdiyne-Ti, CO and O_2 molecules should be coadsorbed on a same metal adatom as catalytic active center. The calculation result indicates that the coadsorption of CO and O_2 would be energetically favorable and advantageous to the LH mechanism. In fact, we have investigated the MEPs of both mechanisms, finding similar transition state structures in the initial step. The LH mechanism firstly arrives at the coadsorption state M·CO·O_2 with lower energy and then goes through the transition state, while in the ER mechanism the reaction directly goes through the transition state with higher energy. Therefore, from the viewpoint of adsorption energy, the LH mechanism is expected to thermodynamically prevail over the ER mechanism. The CO oxidation reaction on graphdiyne-M has been proposed as the following steps:

$$M + O_2 \rightarrow M{\cdot}O_2,\ M{\cdot}O_2 + CO \rightarrow M{\cdot}CO{\cdot}O_2 \quad \text{(Step 1)}$$

$$M{\cdot}CO{\cdot}O_2 \rightarrow M{\cdot}OOCO \quad \text{(Step 2)}$$

$$M{\cdot}OOCO \rightarrow M{\cdot}O + CO_2 \quad \text{(Step 3)}$$

$$M{\cdot}O + CO \rightarrow M + CO_2 \quad \text{(Step 4)}$$

Step 1–3 follow the LH mechanism, including the coadsorption of CO and O_2, the in-situ transformation into an intermediate state and the release of reaction product. After that, one O atom is left on graphdiyne-M and then reacts with a subsequently incoming CO in Step 4.

According to the results, Step 1 should be energetically favorable. The initial state (IS) is composed of clean graphdiyne-M and free CO and O_2 molecules. In the last section, it has been indicated that the graphdiyne-Sc and graphdiyne-Ti would be preferentially adsorbed by O_2. Then, the binding energies $E_b(CO|M{\cdot}O_2)$ of CO on graphdiyne-M·O_2 were calculated. For M = Sc/Ti, the binding energies $E_b(CO|M{\cdot}O_2) = 0.91/0.66$ eV at the level of PBE (Table 2) correspond to the time scales for maintaining the coadsorption

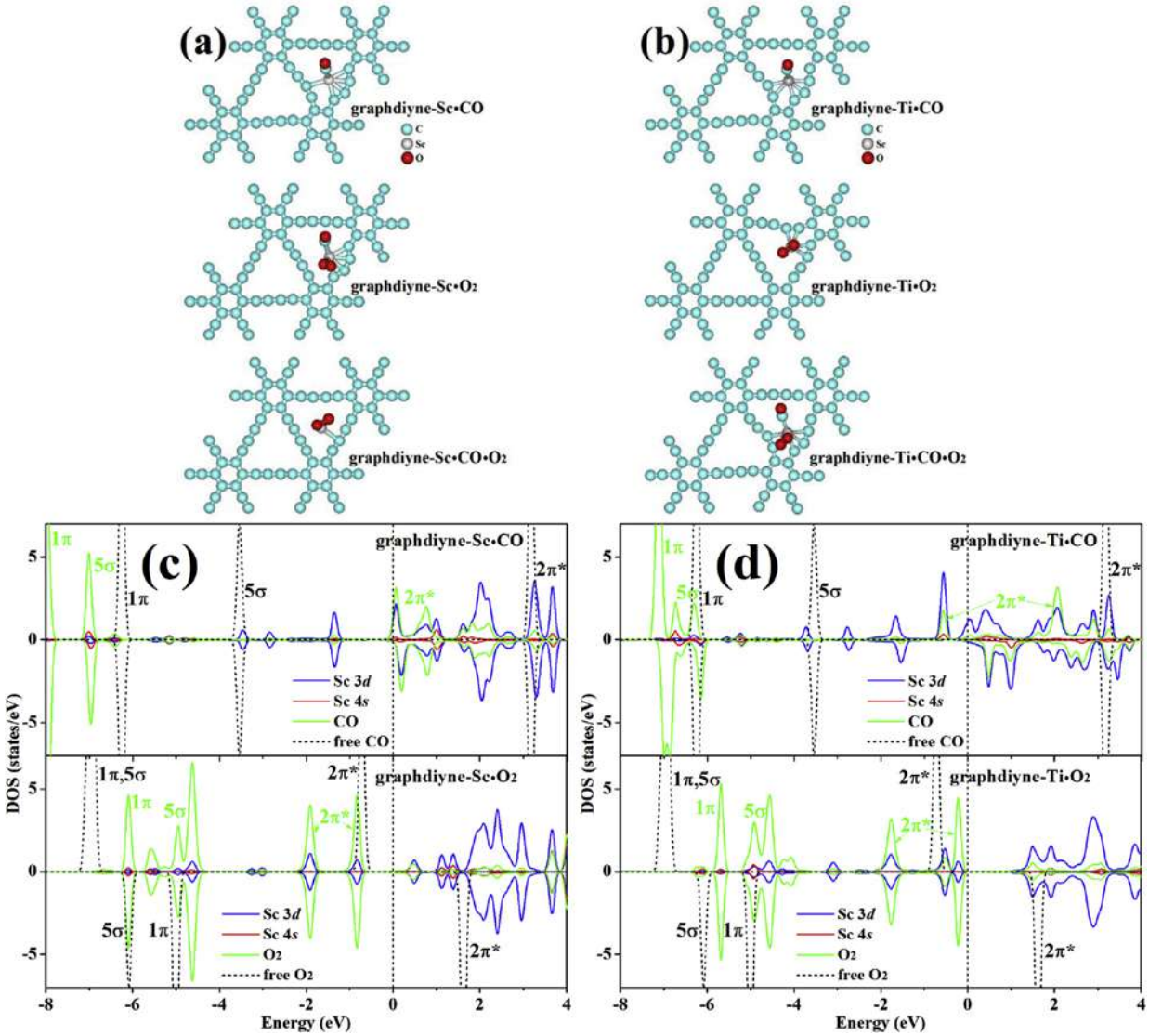

Fig. 2. (a) The most stable configurations of graphdiyne-Sc·CO, graphdiyne-Sc·O_2 and graphdiyne-Sc·CO·O_2. (b) The most stable configurations of graphdiyne-Ti·CO, graphdiyne-Ti·O_2 and graphdiyne-Ti·CO·O_2. (c) The LDOS for graphdiyne-Sc·CO and graphdiyne-Sc·O_2. (d) The LDOS for graphdiyne-Ti·CO and graphdiyne-Ti·O_2. In (c) and (d), the positive and negative LDOS denote the spin-up and spin-down states, respectively. The vertical dashed line indicates the Fermi level. (A colour version of this figure can be viewed online.)

Table 2
The binding energies E_b (in eV) of CO and O_2 molecule. The 1st/2nd column presents E_b of CO/O_2 on the metal adatom M (M = Sc, Ti) anchored on graphdiyne, respectively. The 3rd column presents E_b of CO on M·O_2. The 4th column presents E_b of O_2 on M·CO. All the values are calculated at the level of PBE.

Adatom M	Binding energy (PBE)			
	E_b(CO|M)	E_b(O_2|M)	E_b(CO|M·O_2)	E_b(O_2|M·CO)
Sc	1.17	2.73	0.91	2.47
Ti	1.60	3.69	0.66	2.75

status of about $\tau = \omega^{-1}\exp(E_b(\text{CO}|\text{M}\cdot\text{O}_2)/kT) = 2\times10^2/1\times10^{-2}$ s at $T = 300$ K, respectively. In Fig. 3(a), the configurations of IS and the coadsorption state M·CO·O_2 (MS1) are presented in the first two subfigures. Overall, the energy of MS1, with respect to IS, is $E(\text{MS1}) = -(E_b(\text{CO}|\text{M})+E_b(\text{O}_2|\text{M}\cdot\text{CO})) = -(E_b(\text{O}_2|\text{M})+E_b(\text{CO}|\text{M}\cdot\text{O}_2)) = -3.64/-3.59$ and $-4.35/-4.16$ eV for M═Sc and Ti at the level of PBE/PBE0, each respectively. The coadsorption energy is large enough for stabilizing CO and O_2 together on graphdiyne-M.

In Step 2, the coadsorption state MS1 is transformed into a carbonate-like intermediate state M·OOCO (MS2) via a transition state TS1. The configurations and energies of MS1, TS1 and MS2 are presented in Fig. 3(a) and (b). The energies of TS1 and MS2, with respect to IS, are $E(\text{TS1}) = -2.42/-2.58$ and $-3.74/-3.62$ eV and $E(\text{MS2}) = -6.78/-7.10$ and $-7.65/-7.90$ eV for M = Sc and Ti at the level of PBE/PBE0, each respectively. In Step 2, the barrier E_0(Step 2) = E(TS1)−E(MS1) = 1.22/1.01 and 0.61/0.54 eV at the level of PBE/PBE0, each respectively, needs to be overcome for M═Sc and Ti, corresponding to the typical time scales for Step 2 is about $\tau = \omega^{-1}\exp(E_0(\text{Step 2})/kT) = 3\times10^7/9\times10^4$ and $2\times10^{-3}/1\times10^{-4}$ s at $T = 300$ K. At $T = 500$ K, the reaction time scale is even reduced to about $2\times10^{-2}/2\times10^{-3}$ and $1\times10^{-7}/3\times10^{-8}$ s for M═Sc and Ti at the level of PBE/PBE0, each respectively. Therefore, for M═Ti the reaction could be performed at room temperature, while for M═Sc proper higher temperature is needed for the reaction.

In Step 3, a CO_2 molecule is dissociated from the intermediate MS2. The corresponding configurations and energies are presented in Fig. 3(a) and (b). The system reaches a final state FS composed of

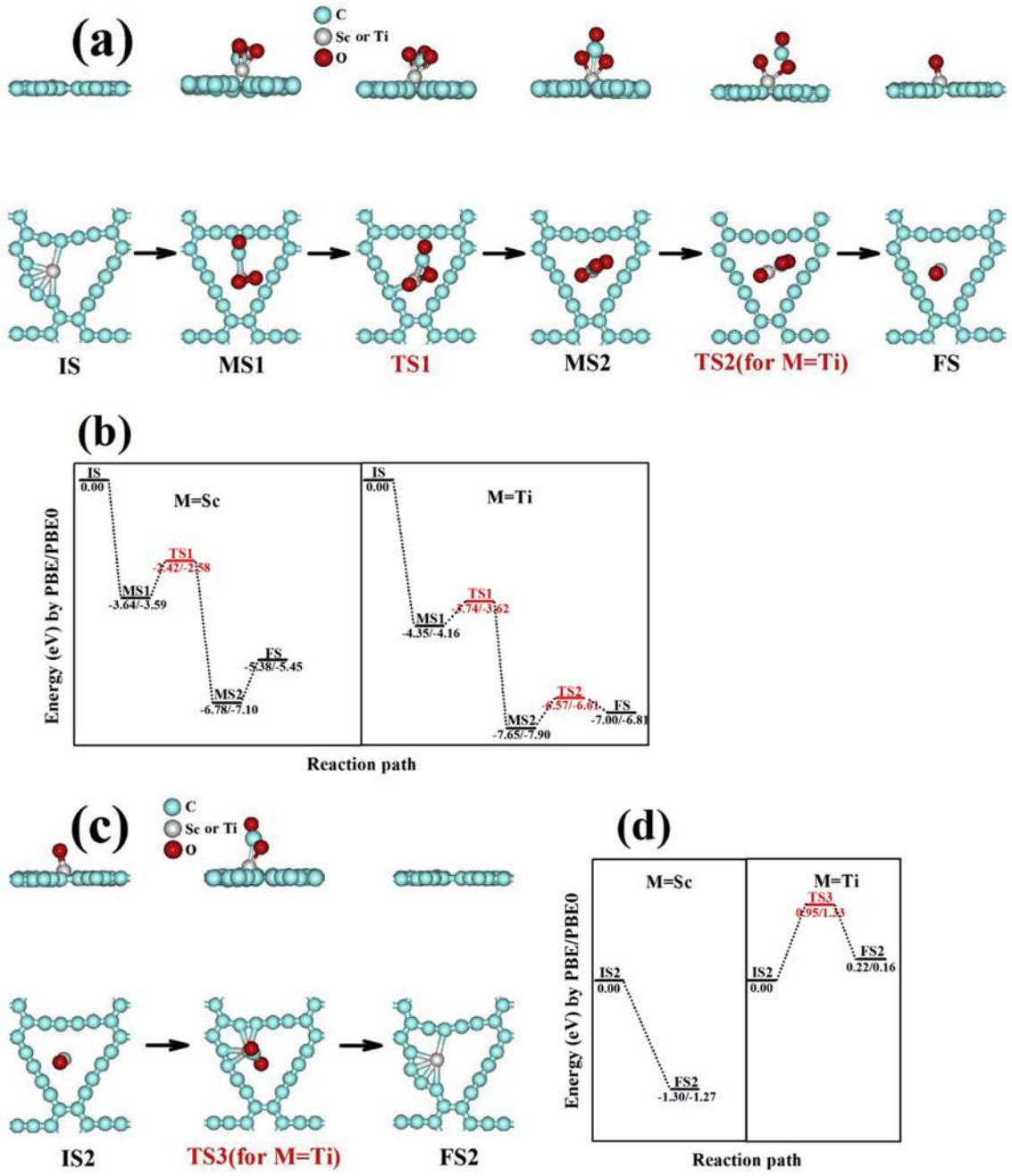

Fig. 3. (a) Top and side views of IS, MS1, TS1, MS2, TS2 (only for M=Ti) and FS along the MEPs of Step 1–3. (b) The energy profile of IS, MS1, TS1, MS2, TS2 (only for M=Ti) and FS along the MEPs of Step 1–3 at the level of PBE/PBE0. (c) Top and side views of IS2, TS3 (only for M=Ti) and FS2 along the MEP of Step 4. (d) The energy profile of IS2, TS3 (only for M=Ti) and FS2 along the MEP of Step 4 at the level of PBE/PBE0. (A colour version of this figure can be viewed online.)

graphdiyne-M·O and free CO_2 molecule. For M = Sc at the level of PBE/PBE0, Step 3 is found barrierless and the system directly varies from MS2 (E(MS2) = −6.78/−7.10 eV) to FS (E(FS) = −5.38/−5.45 eV), with an energy of E(FS)−E(MS2) = 1.40/1.65 eV needed to be overcome, respectively. This energy is too high for Step 3 to be performed at room temperature. However, at T = 600 K, the reaction time scale is reduced to about $\tau = \omega^{-1}\exp((E(\mathrm{FS})-E(\mathrm{MS2}))/kT) = 6 \times 10^{-2}/7 \times 10^{1}$ s at the level of PBE/PBE0, respectively. For M=Ti, Step 3 is achieved via a transition state TS2. At the level of PBE/PBE0, the energies of corresponding configurations are E(MS2) = −7.65/−7.90 eV, E(TS2) = −6.57/−6.61 eV and E(FS) = −7.00/−6.81 eV, respectively. In Step 3, a barrier E_0(Step 3) = E(TS2)−E(MS2) = 1.08/1.29 eV at the level of PBE/PBE0, respectively, is needed to be overcome. At T = 500 K, the reaction time scale is about $\tau = \omega^{-1}\exp(E_0(\text{Step 3})/kT) = 8 \times 10^{-3}/1 \times 10^{1}$ s at the level of PBE/PBE0, respectively. Overall, for M=Sc and Ti, the reaction time scale of Step 3 is short enough and acceptable for catalysis at T = 500 K.

After Step 1–3, the remaining graphdiyne-M·O could react with a new CO molecule in Step 4, releasing a CO_2 molecule. The initial state (IS2) is composed of graphdiyne-M·O and a free CO molecule. The final state (FS2) is composed of clean graphdiyne-M and a free CO_2 molecule. The corresponding configurations and energies are presented in Fig. 3(c) and (d). For M=Sc, the reaction is barrierless.

The energy of the system directly decreases from IS2 (E(IS2) = 0.00 eV) to FS2 (E(FS2) = −1.30/−1.27 eV) at the level of PBE/PBE0, respectively, and therefore the reaction could be quickly performed. For M═Ti, a barrier E_0(TS3) = 0.95/1.33 eV at the level of PBE/PBE0, respectively, is needed to be overcome. This barrier is a bit higher than the same process on graphyne-Fe [58]. At T = 500 K, the reaction time scale is about $\tau = \omega^{-1}\exp(E_0(\mathrm{TS3})/kT) = 4 \times 10^{-4}/3 \times 10^{1}$ s at the level of PBE/PBE0, respectively. Overall, for M═Sc and Ti, Step 4 could be easily achieved at T = 500 K or above.

In summary, Step 1–4 would successfully proceed at T = 600 K or above. For M═Sc/Ti, Step 3/4 acts as the bottleneck of the whole process, respectively. For Ti, the barriers in Step 1–3 are accordingly lower than Sc. However, Step 4 for Sc is barrierless with decreasing energy, while Step 4 for Ti has a barrier. Considering these two factors, the catalytic effects of graphdiyne-Sc and graphdiyne-Ti on CO oxidation may be comparable.

4. Conclusions

In this work, the thermal stability and catalytic ability of Sc and Ti adatoms on single-layer graphdiyne were theoretically investigated by DFT calculations. The results indicate that the **C** sites on graphdiyne surface are the most stable binding sites for Sc and Ti adatoms, with much larger binding energies and much higher migration barriers than on graphene. At room temperature, Sc and Ti adatoms seldom jump from the located **C** site to the neighboring **C** site due to large barrier, preventing the aggregation of these adatoms on graphdiyne. In the presence of Sc and Ti adatoms on graphdiyne, CO in O_2 ambient could be catalytically oxidated by a four-step reaction. The reaction, which is suggested to be efficiently performed at T = 600 K or above, is both energetically and kinetically favorable with stable reaction intermediates and low potential barriers. Overall, with high thermal stability and excellent catalytic ability, Sc and Ti adatoms on single-layer graphdiyne would be excellent catalysts for CO oxidation.

Acknowledgements

This work was supported by the National Natural Science Foundation of China under Grant No. 11304239, and the Fundamental Research Funds for the Central Universities.

References

[1] B. Qiao, A. Wang, X. Yang, L.F. Allard, Z. Jiang, Y. Cui, et al., Single-atom catalysis of CO oxidation using Pt1/FeOx, Nat. Chem. 3 (2011) 634–641.
[2] X.-F. Yang, A. Wang, B. Qiao, J. Li, J. Liu, T. Zhang, Single-atom catalysts: a new frontier in heterogeneous catalysis, Acc. Chem. Res. 46 (2013) 1740.
[3] J. Lin, A. Wang, B. Qiao, X. Liu, X. Yang, X. Wang, et al., Remarkable performance of Ir1/FeOx single-atom catalyst in water gas shift reaction, J. Am. Chem. Soc. 135 (2013) 15314–15317.
[4] H. Wei, X. Liu, A. Wang, L. Zhang, B. Qiao, X. Yang, et al., FeOx-supported platinum single-atom and pseudo-single-atom catalysts for chemoselective hydrogenation of functionalized nitroarenes, Nat. Comm. 5 (2014) 5634.
[5] Y. Tong, H.S. Kim, P.K. Babu, P. Waszczuk, A. Wieckowski, E. Oldfield, An NMR investigation of CO tolerance in a Pt/Ru fuel cell catalyst, J. Am. Chem. Soc. 124 (2002) 468.
[6] J.S. King, A. Wittstock, J. Biener, S.O. Kucheyev, Y.M. Wang, T.F. Baumann, et al., Ultralow loading pt nanocatalysts prepared by atomic layer deposition on carbon aerogels, Nano Lett. 8 (2008) 2405–2409.
[7] E.J. Yoo, T. Okata, T. Akita, M. Kohyama, J. Nakamura, I. Honma, Enhanced electrocatalytic activity of Pt subnanoclusters on graphene nanosheet surface, Nano. Lett. 9 (2009) 2255–2259.
[8] S.R. Brankovic, J.X. Wang, Y. Zhu, R. Sabatini, J. McBreen, R.R. Adžić, Electrosorption and catalytic properties of bare and Pt modified single crystal and nanostructured Ru surfaces, J. Electroanal. Chem. 524–525 (2002) 231–241.
[9] S. Stolbov, A.M. Ortigoza, R. Adzic, T.S. Rahman, High CO tolerance of Pt/Ru nanocatalyst: insight from first principles calculations, J. Chem. Phys. 130 (2009) 124714.
[10] D. Guban, I. Borbath, Z. Paszti, I. Sajo, E. Drotar, M. Hegedus, et al., Preparation and characterization of novel Ti0.7W0.3O2-C composite materials for Pt-based anode electrocatalysts with enhanced CO tolerance, Appl. Catal. B Environ. 174 (2015) 455–470.
[11] Y. Yao, Q. Fua, Y.Y. Zhang, X. Weng, H. Li, M. Chen, et al., Graphene cover-promoted metal-catalyzed reactions, Proc. Natl. Acad. Sci. U. S. A. 111 (2014) 17023–17028.
[12] M. Wei, Q. Fu, Y. Yang, W. Wei, E. Crumlin, H. Bluhm, et al., Modulation of surface chemistry of CO on Ni(111) by surface graphene and carbidic carbon, J. Phys. Chem. C 119 (2015) 13590–13597.
[13] Y.-H. Lu, M. Zhou, C. Zhang, Y.-P. Feng, Metal-embedded graphene: a possible catalyst with high activity, J. Phys. Chem. C 113 (2009) 20156–20160.
[14] K.S. Novoselov, A.K. Geim, S.V. Morozov, D. Jiang, Y. Zhang, S.V. Dubonos, et al., Electric field effect in atomically thin carbon films, Science 306 (2004) 666–669.
[15] K.S. Novoselov, A.K. Geim, S.V. Morozov, D. Jiang, M.I. Katsnelson, I.V. Grigorieva, et al., Two dimensional gas of massless dirac fermions in graphene, Nature 438 (2005) 197–200.
[16] A.K. Geim, K.S. Novoselov, The rise of graphene, Nat. Mater. 6 (2007) 183–191.
[17] M.J. Allen, V.C. Tung, R.B. Kaner, Honeycomb carbon: a review of graphene, Chem. Rev. 110 (2010) 132–145.
[18] A.H. Castro Neto, F. Guinea, N.M.R. Peres, K.S. Novoselov, A.K. Geim, The electronic properties of graphene, Rev. Mod. Phys. 81 (2009) 109.
[19] K.F. Mak, C. Lee, J. Hone, J. Shan, T.F. Heinz, Atomically thin MoS_2: a new direct-gap semiconductor, Phys. Rev. Lett. 105 (2010) 136805.
[20] M. Chhowalla, H.S. Shin, G. Eda, L.-J. Li, K.P. Loh, H. Zhang, The chemistry of two-dimensional layered transition metal dichalcogenide nanosheets, Nat. Chem. 5 (2013) 263–275.
[21] Q.H. Wang, K. Kalantar-Zadeh, A. Kis, J.N. Coleman, M.S. Strano, Electronics and optoelectronics of two-dimensional transition metal dichalcogenides, Nat. Nanotechnol. 7 (2012) 699–712.
[22] J. Ding, Z. Qiao, W. Feng, Y. Yao, Q. Niu, Engineering quantum anomalous/valley Hall states in graphene via metal-atom adsorption: an ab-initio study, Phys. Rev. B 84 (2011) 195444.
[23] K. Li, Y. Li, H. Tang, M. Jiao, Y. Wang, Z. Wu, A density functional theory study on 3d metal/graphene for the removal of CO from H_2 feed gas in hydrogen fuel cells, RSC Adv. 5 (2015) 16394–16399.
[24] Y. Tang, Z. Yang, X. Dai, Trapping of metal atoms in the defects on graphene, J. Chem. Phys. 135 (2011) 224704.
[25] A.V. Krasheninnikov, P.O. Lehtinen, A.S. Foster, P. Pyykkö, R.M. Nieminen, Embedding transition-metal atoms in graphene: structure, bonding, and magnetism, Phys. Rev. Lett. 102 (2009) 126807.
[26] K.T. Chan, J.B. Neaton, M.L. Cohen, First-principles study of metal adatom adsorption on graphene, Phys. Rev. B 77 (2008) 235430.
[27] R.H. Baughman, H. Eckhardt, M. Kertesz, Structure—property predictions for new planar forms of carbon: layered phases containing sp2 and sp atoms, J. Chem. Phys. 87 (1987) 6687–6699.
[28] N. Narita, S. Nagai, S. Suzuki, K. Nakao, Electronic structure of three-dimensional graphyne, Phys. Rev. B 62 (2000) 11146–11151.
[29] N. Narita, S. Nagai, S. Suzuki, K. Nakao, Optimized geometries and electronic structures of graphyne and its family, Phys. Rev. B 58 (1998) 11009–11014.
[30] G. Li, Y. Li, H. Liu, Y. Guo, Y. Lia, D. Zhua, Architecture of graphdiyne nanoscale films, Chem. Commun. 46 (2010) 3256.
[31] M. Long, L. Tang, D. Wang, Y. Li, Z. Shuai, Electronic structure and carrier mobility in graphdiyne sheet and nanoribbons: theoretical predictions, ACS Nano 5 (2011) 2593–2600.
[32] L.D. Pan, L.Z. Zhang, B.Q. Song, S.X. Du, H.-J. Gao, Graphyne- and graphdiyne-based nanoribbons: density functional theory calculations of electronic structures, Appl. Phys. Lett. 98 (2011) 173102–173104.
[33] H.Y. Zhang, Y.Y. Xia, H.X. Bu, X.P. Wang, M. Zhang, Y.H. Luo, et al., Graphdiyne: a promising anode material for lithium ion batteries with high capacity and rate capability, J. Appl. Phys. 113 (2013) 044309.
[34] H. Bu, M. Zhao, H. Zhang, X. Wang, Y. Xi, Z. Wang, Isoelectronic doping of graphdiyne with boron and nitrogen: stable configurations and band gap modification, J. Phys. Chem. A 116 (2012) 3934–3939.
[35] H.X. Bu, M.W. Zhao, A.Z. Wang, X.P. Wang, First-principles prediction of the transition from graphdiyne to a superlattice of carbon nanotubes and graphene nanoribbons, Carbon 65 (2013) 341–348.
[36] D. Malko, C. Neiss, F. Viñes, A. Görling, Competition for graphene: graphynes with direction-dependent dirac cones, Phys. Rev. Lett. 108 (2012) 086804–086807.
[37] Q. Yue, S. Chang, J. Kang, J. Tan, S. Qin, J. Li, Magnetic and electronic properties of α-graphyne nanoribbons, J. Chem. Phys. 136 (2012) 244702–244705.
[38] P. Wu, P. Du, H. Zhang, C. Cai, Graphdiyne as a metal-free catalyst for low-temperature CO oxidation, Phys. Chem. Chem. Phys. 16 (2014) 5640–5648.
[39] Z.-Z. Lin, Q. Wei, X. Zhu, Modulating the electronic properties of graphdiyne nanoribbons, Carbon 66 (2014) 504–510.
[40] Z.-Z. Lin, Graphdiyne as a promising substrate for stabilizing Pt nanoparticle catalyst, Carbon 86 (2015) 301–309.
[41] J.M. Soler, E. Artacho, J.D. Gale, A. García, J. Junquera, P. Ordejón, et al., The SIESTA method for ab initio order-N materials simulation, J. Phys. Condens. Matter 14 (2002) 2745–2779.
[42] N. Troullier, J.L. Martins, Efficient pseudopotentials for plane-wave calculations, Phys. Rev. B 43 (1991) 1993–2006.
[43] J.P. Perdew, K. Burke, M. Ernzerhof, Generalized gradient approximation made simple, Phys. Rev. Lett. 77 (1996) 3865–3868.

[44] S. Grimme, Semiempirical GGA-type density functional constructed with a long-range dispersion correction, J. Comp. Chem. 27 (2006) 1787–1799.
[45] H.J. Monkhorst, J.D. Pack, Special points for brillouin-zone integrations, Phys. Rev. B 13 (1976) 5118.
[46] G. Mills, H. Jónsson, Quantum and thermal effects in H_2 dissociative adsorption: evaluation of free energy barriers in multidimensional quantum systems, Phys. Rev. Lett. 72 (1994) 1124–1127.
[47] G. Mills, H. Jónsson, G.K. Schenter, Reversible work transition state theory: application to dissociative adsorption of hydrogen, Surf. Sci. 324 (1995) 305–337.
[48] G. Henkelman, B.P. Uberuaga, H. Jónsson, A climbing image nudged elastic band method for finding saddle points and minimum energy paths, J. Chem. Phys. 113 (2000) 9901–9904.
[49] J. Paier, R. Hirschl, M. Marsman, G. Kresse, The Perdew-Burke-Ernzerhof exchange-correlation functional applied to the G2-1 test set using a plane-wave basis set, J. Chem. Phys. 122 (2005) 234102.
[50] P.E. Blöchl, Projector augmented-wave method, Phys. Rev. B 50 (1994) 17953–17979.
[51] G. Kresse, D. Joubert, From ultrasoft pseudopotentials to the projector augmented-wave method, Phys. Rev. B 59 (1999) 1758–1775.
[52] G.H. Kresse, J., *Ab initio* molecular dynamics for liquid metals, Phys. Rev. B 47 (1993) 558–561.
[53] G. Kresse, J. Furthmüller, Efficient iterative schemes for *ab initio* total-energy calculations using a plane-wave basis set, Phys. Rev. B 54 (1996) 11169–11186.
[54] J. He, S.Y. Ma, P. Zhou, C.X. Zhang, C. He, L.Z. Sun, Magnetic properties of single transition-metal atom absorbed graphdiyne and graphyne sheet from DFT+U calculations, J. Phys. Chem. C 116 (2012) 26313–26321.
[55] L. Hu, X. Hu, X. Wu, C. Du, Y. Dai, J. Deng, Density functional calculation of transition metal adatom adsorption on graphene, Phys. B 405 (2010) 3337–3341.
[56] M.K. Srivastava, Y. Wang, A.F. Kemper, H.-P. Cheng, Density functional study of gold and iron clusters on perfect and defected graphene, Phys. Rev. B 85 (2012) 165444.
[57] D.W. Ma, T. Li, Q. Wang, G. Yang, C. He, B. Ma, et al., Graphyne as a promising substrate for the noble-metal single-atom catalysts, Carbon 95 (2015) 756–765.
[58] P. Wu, P. Du, H. Zhang, C. Cai, Graphyne-supported single Fe atom catalysts for CO oxidation, Phys. Chem. Chem. Phys. 17 (2015) 1441–1449.
[59] C. Li, J. Li, F. Wu, S.-S. Li, J.-B. Xia, L.-W. Wang, High capacity hydrogen storage in Ca decorated graphyne: a first-principles study, J. Phys. Chem. C 115 (2011) 23221–23225.
[60] S. Weigelt, C. Busse, C. Bombis, M.M. Knudsen, K.V. Gothelf, T. Strunskus, et al., Covalent interlinking of an aldehyde and an amine on a Au(111) surface in ultrahigh vacuum, Angew. Chem. 119 (2007) 9387–9390.
[61] A. Kokalj, Formation and structure of inhibitive molecular film of imidazole on iron surface, Corros. Sci. 68 (2013) 195–203.